chemistry proceedings

MDPI

Proceedings

Assessment of Hectorite/Spring Water Hydrogels as Wound Healing Products †

Fátima García-Villén [1,*], Rita Sánchez-Espejo [2], Ana Borrego-Sánchez [2], Pilar Cerezo [1], Giuseppina Sandri [3] and César Viseras [1,2]

[1] Department of Pharmacy and Pharmaceutical Technology, Faculty of Pharmacy, University of Granada, Campus of Cartuja, 18071 s/n Granada, Spain; mcerezo@ugr.es; cviseras@ugr.es (P.C.); cviseras@ugr.es (C.V.)

[2] Andalusian Institute of Earth Sciences, CSIC-UGR. Avenida de las Palmeras 4, 18100 Armilla, Granada, Spain; ext.risanchez@ugr.es (R.S.-E.); anaborrego@iact.ugr-csic.es (A.B.-S.)

[3] Department of Drug Sciences, Faculty of Pharmacy, University of Pavia, Taramelli street 12, 27100 Pavia, Italy; g.sandri@unipv.it

* Correspondence: fgarvillen@ugr.es; Tel.: +34-608356567

† Presented at the 1st International Electronic Conference on Pharmaceutics, 1–15 December 2020; Available online: https://iecp2020.sciforum.net/.

Published: date

Abstract: Wound healing treatments continue to be a medical challenge, since complications usually lead to chronicization and comorbidities. Natural inorganic ingredients such as clays have demonstrated to exert useful activities in this regard. Hectorite is a smectite clay with desirable rheology due to its layered structure and remarkable swelling capacity. These properties make it appropriate excipient for semisolid systems. Nonetheless, the biocompatibility of natural hectorite has been scarcely addressed, the majority of studies centred in synthetic or functionalized hectorites. The aim of this study was to prepare and characterize a hectorite/spring water hydrogel. The hectorite clay mineral was subjected to a solid-state characterization, while the hydrogel (HTgel@10) was evaluated in terms of rheology, pH and in vitro biocompatibility and wound healing. Results demonstrated that the hectorite possessed a remarkable purity (84% w/w of hectorite), very similar to that of similar pharmaceutical excipients. HTgel@10 showed a non-Newtonian, viscoplastic to pseudoplastic profile and a stable pH for 12 months. In vitro tests reported that the hectorite and the HTgel@10 were biocompatible (cellular viability ≥ 70%). Specifically, the hectorite used in this study was more biocompatible toward fibroblasts than Veegum® HS. The in vitro wound healing test revealed that HTgel@10 was able to favour the wound closure. Therefore, hectorite/spring water hydrogels could be considered as potential wound healing formulations with remarkable stability and safety.

Keywords: inorganic hydrogel; hectorite; biocompatibility; wound healing; rheology

1. Introduction

Clay minerals are widely used in pharmacy due to their versatile physicochemical characteristics, both as actives and excipients. Among all these properties, their swelling capacity is significantly useful in the preparation of semisolid systems, since they are able to form gel-like structures when dispersed in water.

Nowadays, the wound healing process continues to be a challenge for medicine, since complications usually lead to chronicization and comorbidities. Clay minerals have demonstrated to exert useful activities in this regard [1]. In fact, recent studies have demonstrated that hydrogels formed by fibrous clay minerals and natural spring water were able to induce in vitro wound healing

process by affecting both the mobility and the proliferation of fibroblasts [2,3]. In line with these studies, the biocompatibility and wound healing effects of hectorite/spring water hydrogels have been assessed. Hectorite is a smectite clay mineral with a layered structure. Normally, smectite-clay minerals possess desirable rheology properties due to their layered structure and remarkable swelling capacities [4–6], which makes them perfect ingredients in the formulation of semisolid systems. Nonetheless, the biocompatibility of hectorite natural clay mineral has been scarcely addressed. The majority of studies deal with synthetic hectorite-like clay minerals or functionalized natural hectorite [7–13].

The aim of this study was to prepare and fully characterize a hectorite/spring water hydrogel as a wound healing formulation. Apart from a full solid-state characterization of the clay mineral, rheology, pH and in vitro biocompatibility and wound healing (scratch assay) were performed.

2. Experiments

2.1. Materials

A purified clay mineral sample, commercialized as Pangel HT-11 (abbreviated as HT from now on) was used in this study as a solid phase. It was kindly gifted by TOLSA (Madrid, Spain). Medicinal waters from Alicún de las Torres spring source (ALI) was used.

2.2. Solid State Characterization of Hectorite

X-ray powder diffraction (XRPD) and oriented aggregates of HT were carried out using a PANalytical diffractometer, X'Pert Pro model, equipped with an X'Celerator solid-state detector and a spinning sample holder. The diffractogram patterns were recorded using random oriented mounts with CuKα radiation, operating at 45 kV and 40 mA, in the range 4–70°2θ (0.008°2θ step size, 9.73s as scan step time). X-Ray fluorescence analysis (XRF) was performed using a Bruker® S4 Pioneer equipment, with an Rh anode X-ray tube operating at 60 kV and 150 mA.

Shimadzu (mod. TGA-50H) calorimeter was used to perform thermogravimetric analysis (TGA), equipped with a vertical oven and a precision of 0.001 mg. The experiments was performed in 30–950 °C range, atmospheric air (50 mL/min) and a heating rate of 10 °C/min. Differential Scanning Calorimetry (DSC) was performed with a Mettler Toledo (DSC1) apparatus equipped with a FRS5 sensor. DSC analysis was done from 26 °C to 400 °C at 10 °C/min in atmospheric air (50 mL/min).

High Resolution Transmission Electron Microscopy (HR-TEM) was carried out with a FEI TITAN G2 microscope, equipped with Super-X silicon drift windowless energy-dispersive X-ray spectroscopy (EDX) detector. HT was dispersed in ethanol and subjected to ultrasounds prior to its deposition onto a TEM carbon grid (300 mesh). Elemental analysis of the samples were obtained working with a STEM (Scanning Transmission Electron Microscopy) with a High Angle Annular Dark Field (HAADF) detector.

2.2. Hectorite Hydrogel Formulation

Consequently, hydrogels were prepared by dispersing 25 g of HT in 225 mL of ALI, thus obtaining two type of hydrogels, abbreviated as HTgel@10. The turbine high-speed agitator was equipped with a high-traction stirrer head of square mesh working at 8000 rpm for 10 min. The resultant hydrlge was preserved in polyethylene containers in static conditions at room temperature.

2.3. Hydrogel Characterization

2.3.1. Rheology and pH Stability

Rheological characterization of HTgel@10 was performed by a controlled rate viscometer (Thermo Scientific HAAKE, RotoVisco 1) equipped with a plate/plate combination (Ø 20 mm serrated PP20S sensor system). Flow curves were obtained at constant temperature of 25 °C (± 0.5 °C) from 70–800s^{-1}. The rheological characterization (flow curves, apparent viscosities and hysteresis loops)

was performed just after their preparation (0D) and after 48 h (2D), 1, 2, 6 and 12 months (1M, 2M, 6M and 12M). Six replicates were obtained for each sample.

Stability of the HTgel@10 was also monitored through pH, which was studied by a pH-meter Crison pH25+ equipped with a semisolid electrode (5053T). Eight replicates were collected for each sample.

2.3.2. Biocompatibility and Wound Healing Studies

The biocompatibility of HT and HTgel@10 was studied by MTT (3-(4,5-dimethylthiazol-2-yl)-2,5-diphenyltetrazolium bromide) test. Normal human dermal fibroblasts (NHDFs, PromoCell GmbH) were grown in Dulbecco's modified Eagle medium (DMEM, Sigma Aldrich®-Merck), supplemented with 10% fetal bovine serum (FBS, Euroclone), 200 IU/mL penicillin and 0.2 mg/mL streptomycin (PBI International, I). Cultures were kept at 37 °C in a 5% CO_2 atmosphere with 95% of relative humidity and cells were seeded with a density of 10^5 cells/cm^2. HT and HTgel@10 were put in contact with cells for 24 h at 1000, 500, 50 and 5 μg/mL. Eight replicates were assessed for all samples and for the control. After 24 h, the surnatant was withdrawn and replaced by 50 μL of MTT diluted in growth medium (final MTT concentration = 2.5 mg/mL) for 3h. The absorbance was assayed at 570 nm by means of an ELISA plate reader (Imark Absorbance Reader, Bio-rad), 655 nm of reference wavelength. Cell viability was calculated with respect to the viability of the control.

The in vitro wound healing studies were performed in Petri μ-Dish$^{35\ mm,\ low}$ (Ibidi, Giardini), fibroblasts cultured in the same conditions described for MTT. After cell confluence, the silicone inserts were removed and the cells were put in contact with HT and HTgel@10 (50 μg/mL of clay mineral) diluted in DMEM.

3. Results and Discussion

3.1. Solid State Characterization of Hectorite

XRPD of HT showed the typical diffraction pattern of hectorite together with other minor mineral phases (Figure 1). According to the reflections of the diffractogram, feldspar, quartz and calcite are some of the impurities present in the HT sample.

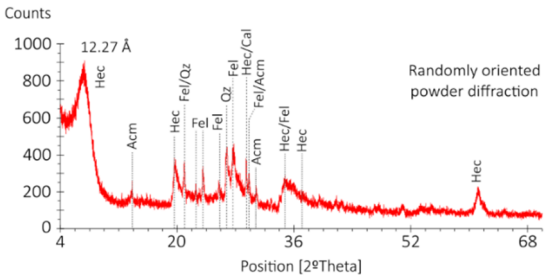

Figure 1. XRPD of HT. Mineral phases identified are included in the diffractogram. Hec: hectorite; Acm: acmite; Fel: potassium feldspar; Cal: calcite.

Oriented mounts (Figure 2) confirmed that the main mineral phase was a smectite since the d001 basal reflection of air-dried diffractogram (14.12 Å) expanded to approximately 16.86 Å with ethylene glycol and then collapsed at 9.72 Å when heated at 550 °C. The combination of XRPD and XRF results (Table 1) made possible the quantification of minor mineral phases. The Si/Mg ratio confirmed that phases such as quartz and feldspar were present, the main one identified by XRPD. Moreover, 5% of calcite was calculated in agreement with the amount of CaO together with the calcite reflections on the diffractogram (3.03Å, Figure 1). Values of iron (Table 1) and reflections at 6.39 and 2.98Å showed the presence of acmite mineral (8%).

Table 1. XRF results of hectorite. The LOI value (Loss of Ignition) accounted for a 9.4% w/w.

Oxides	Amount (%)	Oxides	Amount (%)
SiO_2	53.19	CaO	3.09
Al_2O_3	8.39	Na_2O	5.60
Fe_2O_3	3.42	K_2O	2.83
MnO	0.05	TiO_2	0.37
MgO	13.38	P_2O_5	0.12

Potassium feldspar accounted for 7% (reflections at 3.78 and 3.45Å) and quartz accounted for 4%. Finally, homoionic, sodium hectorite accounted for a 76%. No hectorite monograph is included in the main pharmacopoeias. The most similar pharmaceutical grade clay mineral with which it could be compared is bentonite ("Magnesium aluminium silicate" in USP32-NF27 [14] or "aluminium magnesium silicate" in Ph. Eur. 10th [15]). In comparison with pharmaceutical grade bentonites, such as Veegum® HS (85% of montmorillonite), the pureness of HT is rather high, making it quite acceptable for cosmetic use.

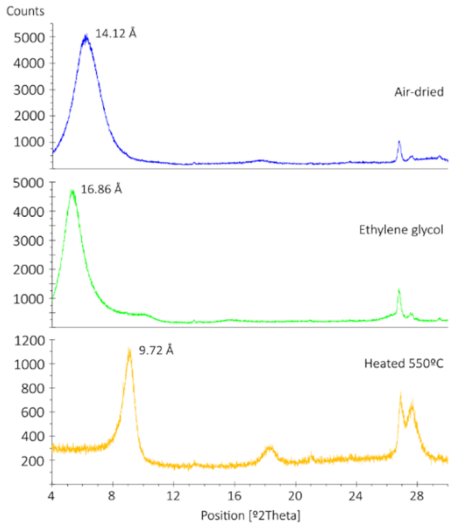

Figure 2. X-ray oriented mounts of HT (air-dried, ethylene glycol and sample heated at 550 °C).

TGA and DSC curves of HT are plotted in Figure 3. The first weight loss in TGA corresponded to free water associated with HT (from 30 to 139 °C). This event coincided with the DSC endothermic peak at 109 °C. Loss of drying for bentonite in the main pharmacopoeias is defined to be between 5 and 15% of weight [14–16], a parameter accomplished by HT. Weigth losss from 140 to 576 °C is ascribed to bound water I and II [17,18]. Dehydroxylation of hectorite happened between 580 to 687 °C and accounted for 1.6% of mass loss (Figure 3B).

HR-TEM confirmed the mineralogical composition. The major part of HT sample corresponded to Figure 4A, in which typical smectite morphology and composition were detected [19–21]. Potassium feldspar crystals were also detected, as showed by the presence of K and Al in Figure 4B. In this image, the feldspar crystal was surrounded by hectorite, which explained the detection of Mg and Na in the spectrum. The proportion of Si, Fe and Na of the crystal analysed in Figure 4C corresponded with the presence of acmite. Spectrum 1 (Figure 4D) is in agreement with the presence of calcite. The spherical morphology of calcite has been previously reported for vaterite [22,23]. The presence of traces of fibrous clay minerals (sepiolite or palygorskite) were also confirmed. A fine, subtle acicular crystal is located to the right of the calcite crystals (spectrum 2, Figure 4D), whose analysis revealed a proportion of Si, Mg and Al in agreement with sepiolite or palygorskite's [2]. The cuboid-shaped crystals in Figure 4D and Figure 4E were identified as rutile [24], which justified the amount of titanium in XRF (Table 1). By the same token, the presence of P_2O_5 corresponded to apatite

traces (Figure 4F). According to XRF, rutile and apatite accounted for approximately 0.4% and 0.3% w/w in HT, respectively.

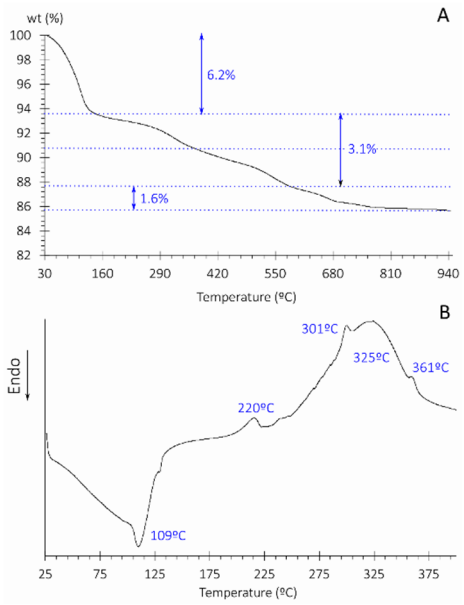

Figure 3. (**A**) TGA analysis and (**B**) DSC analysis of hectorite.

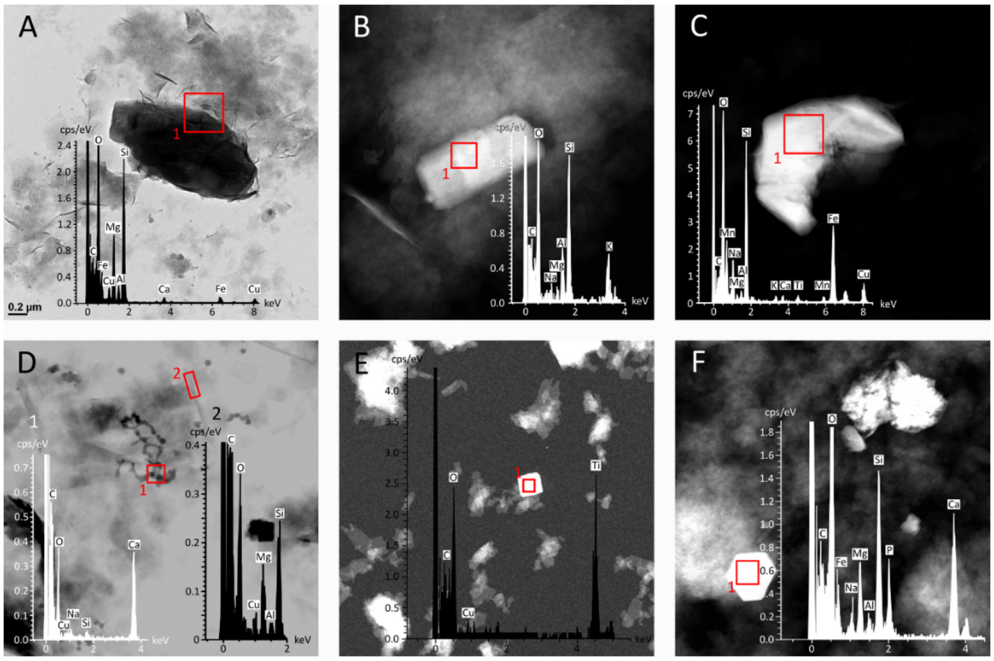

Figure 4. HR-TEM microphotographs of different mineral phases identified in HT sample together with their corresponding EDX analysis. (**A**) hectorite smectite (major part of HT); (B) potassium feldspar mixed with hectorite; (**C**) acmite crystal; (**D**) calcite and sepiolite mixed with hectorite; (**E**) rutile crystal; (**F**) apatite mixed with hectorite. Images B to F were obtained in STEM mode.

3.2. Rheology and pH

Full rheological characterization of HTgel@10 is shown in Figure 5. The hydrogel showed non-Newtonian viscoplastic flow curves that evolved toward pseudoplastic as time passed [5,6,25]. 12M HTgel@10 showed thixotropic hysteresis loops with a characteristic bulge in the upper curve known as spur value that represents a structural breakdown at low shear rates [26]. The apparent viscositiy increased with time, as it can be seen in Figure 5. It is accepted that hectorite disk-like particles are more elongated than those of montmorillonite (MMT), which favoured higher swelling capacities

[27,28]. This fact was confirmed since smaller shear stresses were reported for MMT suspensions at the same solid concentration [29] than HTgel@10. The expansion of the electrical double layer of HT particles prevents the formation of a "house-of-cards" network [30]. Therefore, the individually dispersed suspension make the particles freely flow under stress conditions without forming defined hysteresis loops (0D, 1D, 1M). Thixotropic hysteresis loops appeared from 2M onwards. After 12M the shear stresses decreased with increasing shear rates, something that could be ascribed to a reduction of the electrical double layer of HT particles, thus allowing the formation of a three-dimensional structure that breaks down under stress.

The pH of the HTgel@10 was alkaline, and maintained for 12 months, thus indicating that the formulation was chemically stable. As it can be seen in Table 2, it slightly reduced at the beginning (especially during the first two days due to hydrogel stabilisation) and then maintained around 9.8.

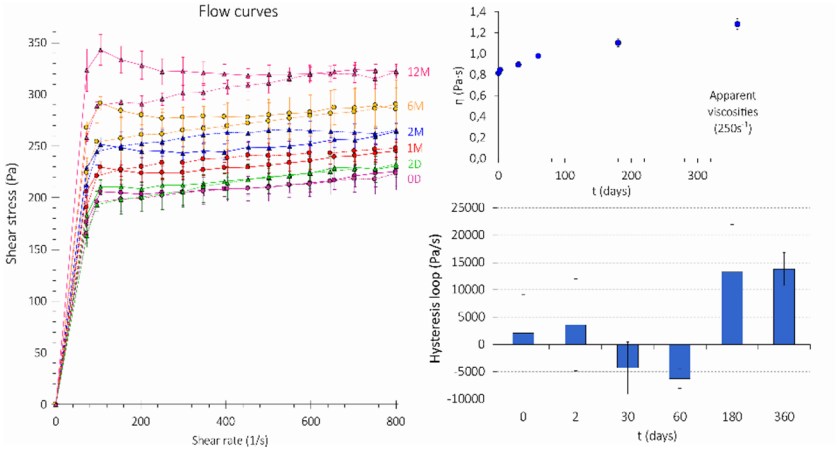

Figure 5. Flow curves, apparent viscositites and hyteresis loops of HTgel@10 (mean values ± s.d.; n = 6 in all cases).

Table 2. Monitoring of HTgel@10 hydrogel.

	0D	2D	30D	2M	6M	12M
pH	10.25 ± 0.013	10.15 ± 0.039	9.96 ± 0.011	9.88 ± 0.013	9.66 ± 0.024	9.88 ± 0.039

3.3. Biocompatibility and Wound Healing

In vitro biocompatibility results of HT and HTgel@10 are reported in Figure 6 (left). Viability (%) was found to be higher than 70% in all cases, which indicates the absence of drastic cellular cytotoxicity within 24h. Significant differences between 1000 µg/mL and GM were found, though the hydrogel reported slightly higher biocompatibility. The precipitation of clay particles over cells could be reduce cellular viability. Nonetheless, Veegum HS® reported to compromise Caco-2 viability from 160 µg/mL of clay (viability ≈50%) [31]. HT demonstrated to be more biocompatible than Veegum HS® (Figure 6, left) [9,11–13,31]. In view of the MTT results, 50 µg/mL was selected as the concentration to evaluate wound healing (Figure 6, right). This test revealed that HTgel@10 performed better results than pure HT. That is, after 48 h, the wounded gap in HT sample was bigger than in HTgel@10 and GM, thus indicating that the semisolid formulation did not interferred with wound healing process.

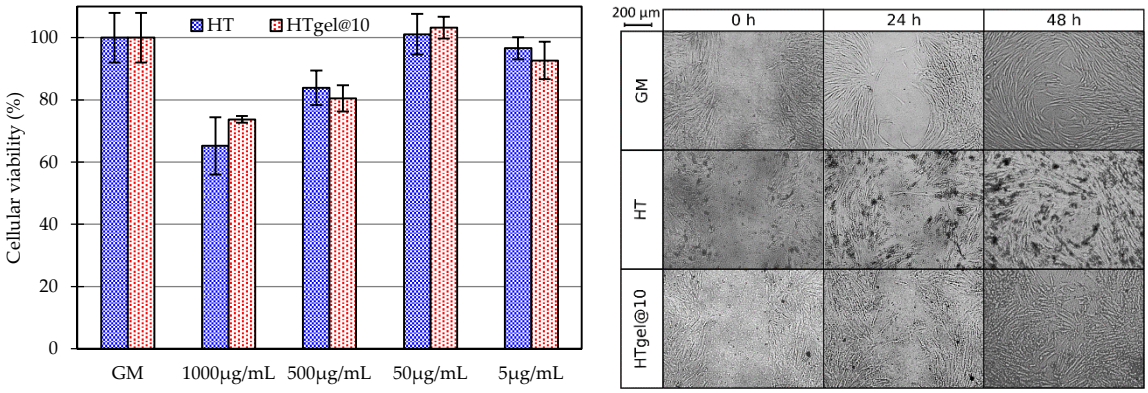

Figure 6. MTT test (**left**) (mean values ± s.e.; n = 8) and wound healing results (**right**). The wound healing was evaluated by using samples at 50 μg/mL. Microphotographs were taken with an inverted optical microscope.

5. Conclusions

In conclusion, the present study demonstrated that the hectorite used in this study could be considered as a pharmaceutical grade excipient in view of its purity, rheological properties and dermal biocompatibility. In fact, this clay is able to form stable hydrogels in a natural spring water with potential wound healing activity, according to the in vitro tests.

Author Contributions: Data curation, F.G.-V.; Funding acquisition, C.V.; Methodology, F.G.-V., R.S.-E., G.S.; Project administration, C.V.; Supervision, R.S.-E., G.S.; Writing—original draft, F.G.-V.; Writing—review & editing, R.S.-E., P.C. All authors have read and agreed to the published version of the manuscript.

Acknowledgments: This research was funded by Ministerio de Ciencia e Innovación, CGL2016–80833-R; Consejería de Economía, Innovación, Ciencia y Empleo, Junta de Andalucía, P18-RT-3786 and Ministerio de Educación, Cultura y Deporte, FPU15/01577.

Conflicts of Interest: The authors declare no conflict of interest.

References

1. García-Villén, F.; Souza, I.M.S.; de Melo Barbosa, R.; Borrego-Sánchez, A.; Sánchez-Espejo, R.; Ojeda-Riascos, S.; Viseras, C. Natural inorganic ingredients in wound healing. *Curr. Pharm. Des.* **2020**, *26*, 621–641.
2. García-Villén, F.; Sánchez-Espejo, R.; López-Galindo, A.; Cerezo, P.; Viseras, C. Design and characterization of spring water hydrogels with natural inorganic excipients. *Appl. Clay Sci.* **2020**, *197*, 105772.
3. García-Villén, F.; Faccendini, A.; Miele, D.; Ruggeri, M.; Sánchez-Espejo, R.; Borrego-Sánchez, A.; Cerezo, P.; Rossi, S.; Viseras, C.; Sandri, G. Wound healing activity of nanoclay/spring water hydrogels. *Pharmaceutics* **2020**, *12*, 1–24.
4. Neaman, A.; Singer, A. Rheology of mixed palygorskite-montmorillonite suspensions. *Clays Clay Miner.* **2000**, *48*, 713–715.
5. Tarchitzky, J.; Chen, Y. Rheology of Sodium-montmorillonite suspensions. *Soil Sci. Soc. Am. J.* **2002**, *66*, 406–412.
6. Aguzzi, C.; Sánchez-Espejo, R.; Cerezo, P.; Machado, J.; Bonferoni, C.; Rossi, S.; Salcedo, I.; Viseras, C. Networking and rheology of concentrated clay suspensions "matured" in mineral medicinal water. *Int. J. Pharm.* **2013**, *453*, 473–479.
7. Haraguchi, K.; Murata, K.; Takehisa, T. Stimuli-responsive nanocomposite gels and soft nanocomposites consisting of inorganic clays and copolymers with different chemical affinities. *Macromolecules* **2012**, *45*, 385–391.
8. Tian, Z.; Zhang, Y.; Liu, X.; Chen, C.; Guiltinan, M.J.; Allcock, H.R. Biodegradable polyphosphazenes containing antibiotics: Synthesis, characterization, and hydrolytic release behavior. *Polym. Chem.* **2013**, *4*, 1826.
9. Huang, K.T.; Fang, Y.L.; Hsieh, P.S.; Li, C.C.; Dai, N.T.; Huang, C.J. Non-sticky and antimicrobial

zwitterionic nanocomposite dressings for infected chronic wounds. *Biomater. Sci.* **2017**, *5*, 1072–1081.
10. Wang, S.; Castro, R.; An, X.; Song, C.; Luo, Y.; Shen, M.; Tomás, H.; Zhu, M.; Shi, X. Electrospun laponite-doped poly(lactic-co-glycolic acid) nanofibers for osteogenic differentiation of human mesenchymal stem cells. *J. Mater. Chem.* **2012**, *22*, 23357–23367.
11. Roozbahani, M.; Kharaziha, M.; Emadi, R. pH sensitive dexamethasone encapsulated laponite nanoplatelets: Release mechanism and cytotoxicity. *Int. J. Pharm.* **2017**, *518*, 312–319.
12. Li, J.; Yang, Y.; Yu, Y.; Li, Q.; Tan, G.; Wang, Y.; Liu, W.; Pan, W. LAPONITE® nanoplatform functionalized with histidine modified oligomeric hyaluronic acid as an effective vehicle for the anticancer drug methotrexate. *J. Mater. Chem. B* **2018**, *6*, 5011–5020.
13. Li, C.; Zhang, W.; Yang, N.; Zhang, Q.S. Fabrication of Organic Hec Nanocomposites Modified with Lysine as a Potential Adsorbent for Bilirubin Removal. *Appl. Biochem. Biotechnol.* **2019**, *188*, 769–786.
14. USP42-NF37. *United States Pharmacopeia and National Formulary*; United States Pharmacopeial Convention: Rockville, MD, USA, 2019.
15. Ph.Eur.9th. *Council of Europe & Convention on the Elaboration of a European Pharmacopoeia*, 9th ed.; Maisonneuve: Sainte-Ruffine, France, 2017.
16. *Handbook of Pharmaceutical Excipients*; Rowe, R.C., Sheskey, P.J., Quinn, M.E., Eds.; Pharmaceutical Press: London, UK, 2009; ISBN 978 0 85369 792 3.
17. Földvári, M. *Handbook of Thermogravimetric System of Minerals and Its Use in Geological Practice*; Gyula, M., Dezsö Simonyi, O.P., Tamás, F., Eds.; Innova-Print Kft.: Budapest, Hungary, 2011; Volume 213; ISBN 978-963-671-288-4.
18. Earnest, C.M. Thermal analysis of hectorite. Part II. Differential thermal analysis. *Thermochim. Acta* **1983**, *63*, 291–306.
19. García-Villén, F.; Faccendini, A.; Aguzzi, C.; Cerezo, P.; Bonferoni, M.C.; Rossi, S.; Grisoli, P.; Ruggeri, M.; Ferrari, F.; Sandri, G.; et al. Montmorillonite-norfloxacin nanocomposite intended for healing of infected wounds. *Int. J. Nanomedicine* **2019**, *14*, 5051–5060.
20. Vazquez, A.; Cyras, V.P.; Alvarez, V.A.; Moran, J.I. Starch/clay nano-biocomposites. *Green Energy Technol.* **2012**, *50*, 287–321.
21. Carrado, K.A.; Csencsits, R.; Thiyagarajan, P.; Seifert, S.; Macha, S.M.; Harwood, J.S. Crystallization and textural porosity of synthetic clay minerals. *J. Mater. Chem.* **2002**, *12*, 3228–3237.
22. Al Omari, M.M.H.; Rashid, I.S.; Qinna, N.A.; Jaber, A.M.; Badwan, A.A. Calcium Carbonate. In *Profiles of Drug Substances, Excipients and Related Methodology*; Academic Press Inc.,Cambridge, MA, USA: 2016; Volume 41, pp. 31–132.
23. Hooley, R.; Brown, A.P.; Kulak, A.N.; Meldrum, F.C.; Brydson, R.M.D. A quantitative evaluation of electron beam sensitivity in calcite nanoparticles. *J. Phys. Conf. Ser.* **2017**, *902*, 89–93.
24. Kobayashi, M.; Kato, H.; Miyazaki, T.; Kakihana, M. Hydrothermal Synthesis of Pseudocubic Rutile-Type Titania Particles. *Ceramics* **2019**, *2*, 56–63.
25. Heller, H.; Keren, R. Rheology of Na-rich montmorillonite suspension as affected by electrolyte concentration and shear rate. *Clays Clay Miner.* **2001**, *49*, 286–291.
26. Barry, B.W. Rheology of pharmaceutical and cosmetic semisolids. In *Advances in Pharmaceutical Sciences*; Bean, H.S., Beckett, A.H., Carless, J. E., Eds.; Academic Press Inc.: London, UK, 1974; Volume. 4, pp. 1–72.
27. Carles, J.E.; Ocran, J. Relations between particle shape, particle interaction and some rheological properties of hectorite dispersions. *J. Pharm. Pharmacol.* **1972**, *24*, 637–644.
28. Bailey, L.; Lekkerkerker, H.N.W.; Maitland, G.C. Smectite clay-inorganic nanoparticle mixed suspensions: Phase behaviour and rheology. *Soft Matter* **2015**, *11*, 222–236.
29. Viseras, C.; Meeten, G.H.; Lopez-Galindo, A. Pharmaceutical grade phyllosilicate dispersions: The influence of shear history on floc structure. *Int. J. Pharm.* **1999**, *182*, 7–20.
30. Kimura, H.; Sakurai, M.; Sugiyama, T.; Tsuchida, A.; Okubo, T.; Masuko, T. Dispersion state and rheology of hectorite particles in water over a broad range of salt and particle concentrations. *Rheol. Acta* **2011**, *50*, 159–168.

31. Salcedo, I.; Aguzzi, C.; Sandri, G.; Bonferoni, M.C.; Mori, M.; Cerezo, P.; Sánchez, R.; Viseras, C.; Caramella, C. In vitro biocompatibility and mucoadhesion of montmorillonite chitosan nanocomposite: A new drug delivery. *Appl. Clay Sci.* **2012**, *55*, 131–137.
32. Su, Y.; Liao, J.L.; Wang, F. Effect of Orient House-Chuen, a concentrate of deep underground mineral spring water, on proliferation and tyrosinase activity of melanocytes. *Chin. J. Biol.* **2010**, *23*, 964–966.